Available online at www.sciencedirect.com

ScienceDirect

Mendeleev Commun., 2019, **29**, 666–668

Mendeleev Communications

Influence of the electronic state of the metals in Fe–Pt/SiO_2 catalysts on the performance of hydrogenation of phenylacetylene

Anastasiya A. Shesterkina,*[a] Olga P. Tkachenko,[a] Elena V. Shuvalova,[a] Gennady I. Kapustin,[a] Vladimir B. Kazansky[a] and Leonid M. Kustov[a,b]

[a] *N. D. Zelinsky Institute of Organic Chemistry, Russian Academy of Sciences, 119991 Moscow, Russian Federation. Fax: +7 499 135 5328; e-mail: anastasiia.strelkova@mail.ru*

[b] *Department of Chemistry, M. V. Lomonosov Moscow State University, 119991 Moscow, Russian Federation*

DOI: 10.1016/j.mencom.2019.11.021

Iron-modified platinum bimetallic system, 1% Pt–1% Fe/SiO_2, provides selective liquid-phase hydrogenation of phenylacetylene into styrene at 70 °C and 5 atm. This effect is attributed to the electron enrichment of the Pt surface atoms due to a charge transfer from Fe to Pt or contact interactions between these two metals, as indicated by XPS and DRIFTS-CO.

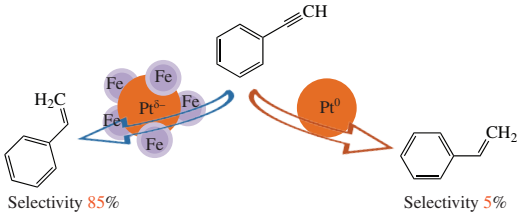

Bimetallic catalysts possess unique properties differing from those of monometallic ones. The high catalytic activity of bimetallic systems appears due to many factors, such as the structure, size and dispersion of nanoparticles, the method of synthesis and conditions of thermal treatments and reduction, the metal ratio, as well as the nature of the support.[1–3] The conditions for the synthesis of bimetallic catalysts can impact metal–metal interaction regulating charge transfer within the metals, which, in turn, provides tuning in component electronegativity.[4,5–8] Catalytic properties of such bimetallic systems are usually different from those of monometallic catalysts; moreover, application of metals on a carrier can seriously influence the charge transfer.[7] The effect of the charge transfer on catalytic properties is described mostly for bimetallic nanoparticles containing noble (Pt, Au, Rh, Ru) and non-noble (Cu, Ni, Zn) metals.[8–10] However, the phenomenon of charge transfer in Fe–M systems and its influence on catalytic properties have been scarcely investigated. The present work was focused on the synthesis of the supported bimetallic Fe–Pt/SiO_2 catalysts,[†] the study of samples by XRD, TPR-H_2, DRIFTS-CO, XPS, TEM and the investigation of catalytic properties in the model hydrogenation of phenylacetylene. The hydrogenation of unsaturated compounds is of great practical importance.[11]

The reducibility of the calcined samples was estimated by TPR as described previously[12,13] (Figure 1). The results indicate that the presence of platinum in the bimetallic calcined catalyst contributes to the reduction of iron oxides at lower temperatures. According to reported data,[14] platinum reduction occurs in the range of 100–280 °C with a maximum at 200 °C in a sample containing 1% Pt deposited on SiO_2 using a similar platinum precursor. Therefore, the presence of iron oxide also contributes to the reduction of platinum at lower temperatures since for the bimetallic sample the peak of platinum reduction was found at 100 °C. The deconvolution of the TPR curve for the calcined 1% Pt–1% Fe/SiO_2–300C catalyst is shown in Figure S1 (see Online Supplementary Materials). The peaks with the maxima at 101 and 160 °C can be attributed to the reduction of platinum oxides to metallic Pt. The peak with a maximum at 230 °C can be assigned to the reduction of Fe_2O_3 to Fe_3O_4, the peak with a maximum at 360 °C corresponds to the reduction of Fe_3O_4 to FeO and the peak with a maximum at 510 °C can be ascribed to further reduction to Fe^0.[15,16] Thus, it can be concluded that the oxide phases of iron and platinum in the bimetallic 1% Pt–1% Fe/SiO_2–C–H sample are completely reduced under hydrogen at 480 °C after calcination.

The state of the metals in the catalysts was estimated using the DRIFTS-CO spectroscopic study (Figures 2 and S2). Several bands are visible in the spectrum of calcined catalyst 1% Pt–1% Fe/SiO_2–C (see Figure S2). The band at 2351 cm^{-1} characterizes adsorbed CO_2 and indicates CO oxidation on Fe^{3+} sites that are thereby reduced to Fe^{2+} ions.[17] The band at

[†] Supported bimetallic 1% Pt–1% Fe catalysts were prepared by simultaneous incipient wetness impregnation of a SiO_2 carrier (Chimmed, Russia, S_{BET} = 108 m^2 g^{-1}, V_{por} = 1.05 cm^3 g^{-1}, D_{por} = 26 nm) with aqueous solutions of metal precursors $Fe(NO_3)_3$ (0.205 M) and H_2PtCl_6 (0.100 M) for 2 h. The impregnated samples were dried at 110 °C for 12 h and then calcined in air at 300 °C for 3 h. The calcined catalysts were reduced in H_2 flow at 480 °C for 3 h and then cooled to 20 °C. Acetone was introduced into the reactor with the reduced sample to exclude the contact with oxygen inside the reactor and to prevent oxidation of Fe nanoparticles. The synthesized catalysts were designated as 1% Pt–1% Fe–C for the calcined samples and as 1% Pt–1% Fe–C–H for the samples reduced in H_2. The reference monometallic 1% Fe/SiO_2 and 1% Pt/SiO_2 catalysts were prepared similarly.

Catalytic properties of the samples were studied in phenylacetylene hydrogenation at 70 °C in H_2 (5 atm) in ethanol (15 ml) (50 mg of catalysts, 0.16 M phenylacetylene, molar ratio substrate: ΣM was 180 : 1).

Diffuse-reflectance IR (DRIFT) spectra were recorded at room temperature in the range of 6000–400 cm^{-1} with a step of 4 cm^{-1} on a NICOLET 'Protege' 460 spectrometer supplied with a diffuse-reflectance unit. CaF_2 powder was used as a standard. CO adsorption was carried out at room temperature and 40 Torr CO. XPS were recorded on an ES-2403 spectrometer with a PHOIBOS 100 MCD analyzer. The spectrometer was pre-calibrated by the binding energy of Au $4f_{7/2}$ = 84.0 eV and Ni $2p_{3/2}$ = 852.7 eV. Kα radiation of the anode Mg (1253.6 eV) at a power of 10 KV × 20 mA was used as an X-ray source.

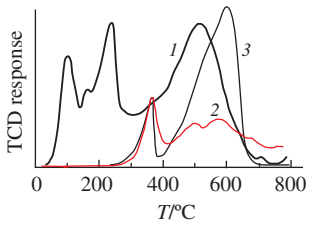

Figure 1 TPR-H_2 profiles of (*1*) 1% Pt–1% Fe/SiO_2–C and (*2*) 1% Fe/SiO_2 samples as well as (*3*) Fe_2O_3 reference.

2127 cm^{-1} is assigned to stretching vibrations of the C≡O bond in CO adsorbed on divalent iron cations (Fe^{2+}–CO).[18] The intensity of this band gradually decreases without shift during thermodesorption. The band at 2097 cm^{-1} is attributed to linear forms of carbonyls on metallic platinum (Pt^0–CO). The intensity of this band decreases during the CO desorption and it is shifted to 2086 cm^{-1}, which may indicate a strong interaction of the supported metals with each other.[18,19]

DRIFT-CO spectrum of the reduced 1% Pt–1% Fe/SiO_2–C–H catalyst contains five bands at 2160, 2031, 1980, 1912 and 1867 cm^{-1} (see Figure 2). The band at 2160 cm^{-1} characterizes linear carbonyls on divalent iron cations (Fe^{2+}–CO). The bands at 2031 and 1867 cm^{-1} are attributed to linear (Pt^0–CO) and bridged (Pt^0–CO–Pt^0) carbonyls on metallic platinum, respectively. DRIFT spectroscopic studies with adsorbed CO revealed the presence of Fe^0 on the surface of the reduced sample since the bands observed at 1980 and 1912 cm^{-1} correspond to linear (Fe^0–CO) and bridged carbonyls (Fe^0–CO–Fe^0).[4,20–22] According to DRIFTS-CO, the platinum in the monometallic 1% Pt/SiO_2–H system has been completely reduced as evidenced by one band at 2088 cm^{-1} (Pt^0–CO). Comparison of DRIFTS-CO on the reduced monometallic and bimetallic samples shows that the band of linear carbonyls (Pt^0–CO) in the spectrum of the bimetallic sample is shifted towards lower frequencies and the intensity of this band decreases, which indicates a modification of platinum, in particular, an increase in the electron density on platinum and the appearance of a partially negatively charged particle ($Pt^{\delta-}$) in the bimetallic catalyst. Iron in the bimetallic sample is present both in the oxidized and in the reduced states (*cf.* refs. 4, 23). DRIFTS-CO results are in accordance with XPS data indicating that platinum exists as electron-modified metal particles of a low dispersion with an increased electron density due to the influence of the nearest electron-deficient Fe atoms.

The study of the reduced bimetallic sample by XRD showed the presence of only reflexes of the SiO_2 carrier, which testifies to the formation of X-ray amorphous phases of both Fe and Pt, high dispersion of the deposited metals and small particle size (Figure S3). TEM images indicate that mean size of nanoparticles in bimetallic sample 4–5 nm (Figure S4). It should be noted that the average particle size in a monometallic sample is slightly higher than 5–6 nm.

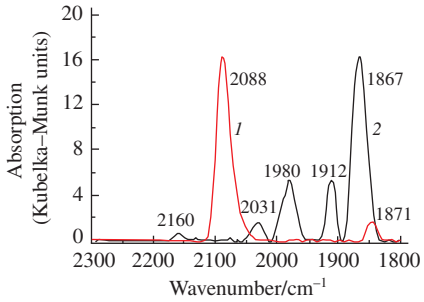

Figure 2 DRIFT-CO spectra of reduced (*1*) 1% Pt/SiO_2–H and (*2*) 1% Pt–1% Fe/SiO_2–C–H catalysts.

Table 1 Initial hydrogenation rates (r_0) and selectivity (S_{St}) to styrene at phenylacetylene conversion of 50 and 95%.

Catalyst	$r_0{}^a$/s^{-1}	t^{50}/min	S_{St}^{50} (%)	t^{95}/min	S_{St}^{95} (%)
1% Pt/SiO_2–H	0.45	15	75	32	5
1% Fe/SiO_2–H	0.0089	–	–	–	–
1% Pt–1% Fe/SiO_2–C–H	0.015	135	80	375	85

[a] Moles of converted PhC≡CH per mole of metal within one second.

The XPS results reveal that platinum in the surface layers of the monometallic sample is present in a metallic state (71.2 eV) (see Online Supplementary Materials, Table S1).[24,25] A lower binding energy of Pt $4f_{7/2}$ electrons (70.8 eV) was observed for the bimetallic 1% Pt–1% Fe/SiO_2–C–H sample, which indicates an increased electron density on Pt atoms. This effect is possible due to the transfer of electrons from Fe to Pt in bimetallic particles.[4,25,26] The concentration of platinum Pt/Si in the surface layers (0.0022) of the monometallic catalyst differs from the volume concentration (0.0036), which may indicate a non-uniform distribution of platinum over the volume of the monometallic catalyst. This behavior may be caused by both migration of platinum into the depth of sample and sintering of the particles during the reduction process. The volume atomic ratio Pt/Si in the bimetallic catalyst was 0.0017, which may be due to the formation of bimetallic Fe–Pt particles with a core (Pt)–shell (Fe) structure. The energy position of the Fe $2p_{3/2}$ line (710.9 eV) indicates that iron in the surface layers is in the oxidation state of Fe^{3+},[27–30] which can result from partial oxidation of the sample during its storage.

The catalytic activity of the prepared mono- and bimetallic samples in liquid-phase hydrogenation of phenylacetylene under mild conditions is summarized in Table 1 and Figures 3, 4. All the synthesized catalysts were catalytically active under the reaction conditions (70 °C, 5 atm), however the activity of the reduced monometallic 1% Fe/SiO_2 catalyst was relatively low (see Figure 3). The highest rates of hydrogenation are achieved in the presence of the monometallic 1% Pt/SiO_2 catalysts. The monometallic platinum samples showed a high selectivity to styrene (75%) at the 50% conversion of the substrate (see Figure 4). However, at the higher conversion, its selectivity declines to 5%. According to the data given in Table 1, unlike the monometallic platinum catalyst, the reduced bimetallic 1% Pt–1% Fe/SiO_2–C–H catalyst exhibited the highest selectivity to styrene (80–85%) both at the 50% and full conversion.

Thus, the strong contact interaction between Pt and Fe and the charge transfer from Fe to Pt in a bimetallic particle, proven by XPS, TPR and DRIFTS-CO methods, provide both high selectivity of the bimetallic catalyst and increased activity in liquid-phase hydrogenation of triple C–C bonds in comparison with monometallic systems.

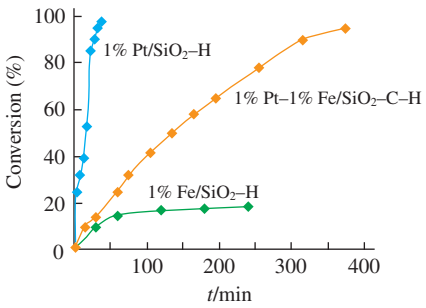

Figure 3 The dependence of conversion of phenylacetylene on the reaction time for different catalysts.

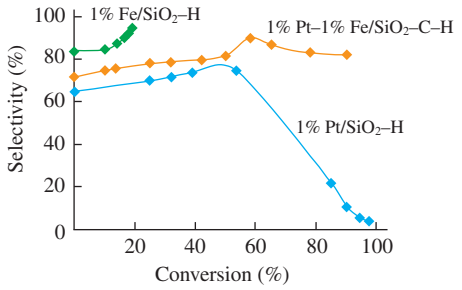

Figure 4 The dependence of the selectivity to styrene on the phenylacetylene conversion for different catalysts.

The authors are grateful to Dr. I. Mishin for the study of samples of catalysts by XRD analysis.

Online Supplementary Materials

Supplementary data associated with this article can be found in the online version at doi: 10.1016/j.mencom.2019.11.021.

References

1 K. Adamska, J. Okal and W. Tylus, *Appl. Catal., B*, 2019, **246**, 180.
2 I. S. Mashkovsky, P. V. Markov, G. O. Bragina, G. N. Baeva, A. V. Rassolov, A. V. Bukhtiyarov, I. P. Prosvirin, V. I. Bukhtiyarov and A. Yu. Stakheev, *Mendeleev Commun*., 2018, **28**, 152.
3 I. S. Mashkovsky, N. S. Smirnova, P. V. Markov, G. N. Baeva, G. O. Bragina, A. V. Bukhtiyarov, I. P. Prosvirin and A. Yu. Stakheev, *Mendeleev Commun*., 2018, **28**, 603.
4 A. Siani, O. S. Alexeev, G. Lafaye and M. D. Amiridis, *J. Catal*., 2009, **266**, 26.
5 X. Gao, Z. Tan, K. Hidajat and S. Kawi, *Catal. Today*, 2017, **281**, 250.
6 P. Wu, Y. Cao, Y. Wang, W. Xing, Z. Zhong, P. Bai and Z. Yan, *Appl. Surf. Sci*., 2018, **457**, 580.
7 A. Vicente, G. Lafaye, C. Especel, P. Marécot and C. T. Williams, *J. Catal.*, 2011, **283**, 133.
8 G. Kyriakou, M. B. Boucher, A. D. Jewell, E. A. Lewis, T. J. Lawton, A. E. Baber, H. L. Tierney, M. Flytzani-Stephanopoulos and E. C. Sykes, *Science*, 2012, **335**, 1209.
9 W. T. Min, H. Emerich and J. A.van Bokhoven, *J. Phys. Chem. C*, 2011, **115**, 8457.
10 A. J. Pamphile-Adrián, P. P. Florez-Rodriguez, M. H. M. Pires, G. Perez and F. B. Passos, *Catal. Today*, 2017, **289**, 302.
11 E. A. Karakhanov, A. L. Maximov and A. V. Zolotukhina, *Mol. Catal.*, 2019, **469**, 98.
12 O. A. Kirichenko, V. D. Nissenbaum, G. I. Kapustin and L. M. Kustov, *Thermochim. Acta*, 2009, **494**, 35.
13 O. A. Kirichenko, G. I. Kapustin, V. D. Nissenbaum, I. V. Mishin and L. M. Kustov, *J. Therm. Anal. Calorim*., 2014, **118**, 749.
14 P. Reyes, G. Pecchi, M. Morales and J. L. G. Fierro, *Appl. Catal., A*, 1997, **163**, 145.
15 O. Kirichenko, G. Kapustin, V. Nissenbaum, A. Strelkova, E. Shuvalova, A. Shesterkina and L. Kustov, *J. Therm. Anal. Calorim*., 2018, **134**, 233.
16 C. Sun, D. Mao, L. Han and J. Yu, *Catal. Commun*., 2016, **84**, 175.
17 A. A. Shesterkina, E. V. Shuvalova, E. A. Redina, O. A. Kirichenko, O. P. Tkachenko, I. V. Mishin and L. M. Kustov, *Mendeleev Commun*., 2017, **27**, 512.
18 A. A. Davydov, *Molecular Spectroscopy of Oxide Catalyst Surfaces*, ed. N. T. Sheppard, Wiley, Chichester, 2003.
19 N. Sheppard and T. T. Nguyen, in *Advances in Infrared and Raman Specroscopy*, eds. R. E. Hester and R. J. H. Clark, Heyden & Sons, London, 1978, vol. 5, ch. 2, pp. 67–134.
20 C. Johnson, N. Jorgensen and C. H. Rochester, *J. Chem. Soc., Faraday Trans*., 1988, **84**, 309.
21 C. Mihut, C. Descorme, D. Duprez and M. D. Amiridis, *J. Catal*., 2002, **212**, 125.
22 A. A. Davydov and N. Coville, *Russ. Chem. Bull.*, 1995, **44**, 1866 (*Izv. Akad. Nauk, Ser. Khim.*, 1995, 1946).
23 A. Fukuoka, T. Kimura, N. Kosugi, H. Kuroda, Y. Minai, Y. Sakai, T. Tominaga and M. Ichikawa, *J. Catal*., 1990, **126**, 434.
24 C. D. Wagner, W. M. Riggs, L. E. Davis, J. F. Moulder and G. E. Muilenberg, *Handbook of X-ray Photoelectron Spectroscopy*, Perkin-Elmer, Eden Prairie, MN, 1979.
25 K. M. Minachev and E. S. Shpiro, *The Catalyst Surface: Physical Methods of Studying*, CRC Press, Boston, 1990.
26 R. P. Doherty, J.-M. Krafft, C. Méthivier, S. Casale, H. Remita, C. Louis and C. Tomas, *J. Catal*., 2012, **287**, 102.
27 B. J. Auten, H. F. Lang and B. D. Chandler, *Appl. Catal., B*, 2008, **81**, 225.
28 T. J. Pan, Y. S. Li, Q. Yang, D. M. Korotin, E. Z. Kurmaev, M. Sanchez-Pasten, I. S. Zhidkov and S. O. Cholakh, *J. Alloys Compd*., 2018, **740**, 887.
29 N. Sgrolli, N. Imlyhen, J. Volkman, A. M. Raspolli-Galletti and P. Serp, *Mol. Catal*., 2017, **438**, 143.
30 X. Shi, H. Yu, S. Gao, X. Li, H. Fang, R. Li, Y. Li, L. Zhang, X. Liang and Y. Yua, *Fuel*, 2017, **210**, 241.

Received: 16th May 2019; Com. 19/5925